Nonlinear 3D M3D-C1 Simulations of Tokamak Plasmas Crossing a MHD Linear Stability Boundary

S. Jardin[1], N. Ferraro[1], J. Breslau[1], J. Chen[1], A. Fil[1], S. Gerhardt[1], S. Hudson[1], E. Kolemen[1], I. Krebs[1,2], C. Myers[1], D. Pfefferle[1], S. Seol[3], M. Shephard[3], B. Tobias[1], F. Zhang[3]

[1]Princeton Plasma Physics Laboratory, P.O. Box 451, Princeton, NJ 08543
[2]Max-Planck-Institut für Plasmaphysik, Garching, Germany
[3]Rensselaer Polytechnic Institute, Troy, NY

email: jardin@pppl.gov

Abstract. Understanding the difference between hard and soft limits is crucial for effective disruption prediction and avoidance in tokamak plasmas. We present several computational examples of both hard and soft beta limits. In the examples presented here, we begin the simulation with the plasma stable to all modes. During the simulation the plasma crosses a stability boundary due to evolving profiles, loss of control, or injection of mass, energy, and or flux. This can lead to saturation or disruption. Effective real-time disruption prediction requires that we can distinguish between the two.

1.0 Introduction:

The goal of the present work is to give an overview of the work our group is doing in the area of *nonlinear* disruption prediction. We seek to better understand and develop a predictive capability for when approaching and crossing a MHD linear instability boundary leads to a thermal quench and subsequent disruption (hard limit), and when it just leads to increased transport or small amplitude oscillations (soft limit). Recent advances in implicit numerical algorithms for solving the 3D extended magneto-hydrodynamic equations in strongly magnetized plasmas have enabled massively parallel simulations of the internal global dynamics of tokamaks that can use very large time steps which allow one to span the timescales of ideal MHD stability, magnetic reconnection, and particle, energy, and momentum transport. M3D-C1 [1] is a flexible initial value code system that can solve a range of plasma models including 2-variable reduced MHD, 4-variable reduced MHD, full resistive single fluid MHD, and 2-fluid extended MHD. It employs high-order finite elements with C^1 continuity in all three spatial dimensions and uses a split-implicit time advance. An internal Grad-Shafranov equilibrium solver computes or resolves the initial equilibrium (eg. from a geqdsk file) on the finite-element grid. It has options for 2D nonlinear, 3D linear and 3D nonlinear computations. In addition, a new multi-region and flexible adaptive meshing capability [2] allows efficient simulation of highly localized modes, and also simulation of the self-consistent interaction of the plasma with a resistive wall [3].

2.0 Hard disruptive limits:

2.1 Current Ramp-down Disruption:

In NSTX discharge 129922, the applied loop voltage was suddenly reversed at the end of the discharge, causing the plasma to disrupt. M3D-C1 full MHD 3D simulations of this event show that as the current reverses near the outside, edge ballooning modes with toroidal mode number (10, 9, 11) first become unstable. As these grow, they drive both higher and lower mode numbers, and this process continues until stochastic processes cause a thermal quench

which subsequently causes a current quench. We see in Figure 1 (right top) a graph of the kinetic energy in select toroidal modes (n). M3D-C1 uses Hermite cubic finite elements

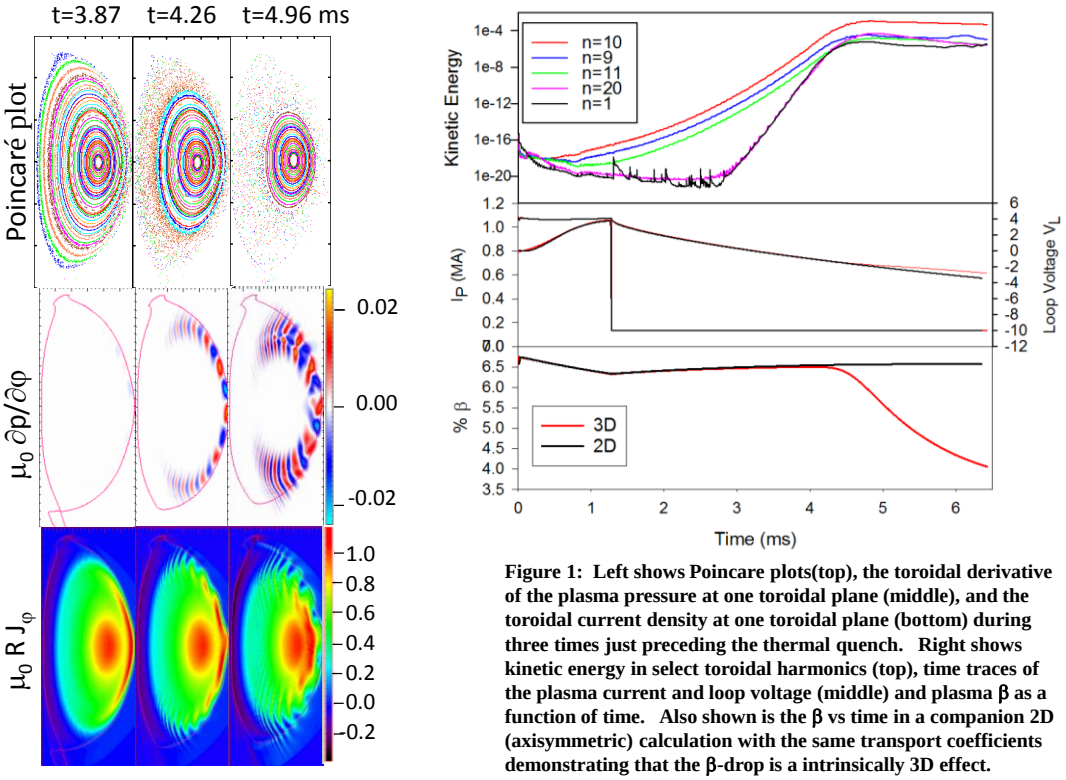

Figure 1: Left shows Poincare plots(top), the toroidal derivative of the plasma pressure at one toroidal plane (middle), and the toroidal current density at one toroidal plane (bottom) during three times just preceding the thermal quench. Right shows kinetic energy in select toroidal harmonics (top), time traces of the plasma current and loop voltage (middle) and plasma β as a function of time. Also shown is the β vs time in a companion 2D (axisymmetric) calculation with the same transport coefficients demonstrating that the β-drop is a intrinsically 3D effect.

in the toroidal direction, 64 in this calculation, which should allow accurate computation of modes up to n=20. Numerical convergence studies show that the solution is well converged up until about 5 ms, when the nonlinearly driven toroidal harmonics with n > 20 are not well represented. We are presently exploring using higher-order dissipative terms in the equations that will damp these very high toroidal harmonics and allow the computation to proceed. Figure 1 (left) shows Poincaré plots (top), the toroidal derivative of the plasma pressure at one toroidal plane (middle) and the toroidal current density at one toroidal plane (bottom) during three times just proceeding the induced thermal quench. It is seen that the unstable eigenfunction initially resides at the plasma boundary as the current starts to reverse. As time goes on, it affects more of the plasma, causing the volume of the stochastic region to increase and a thermal quench to occur.

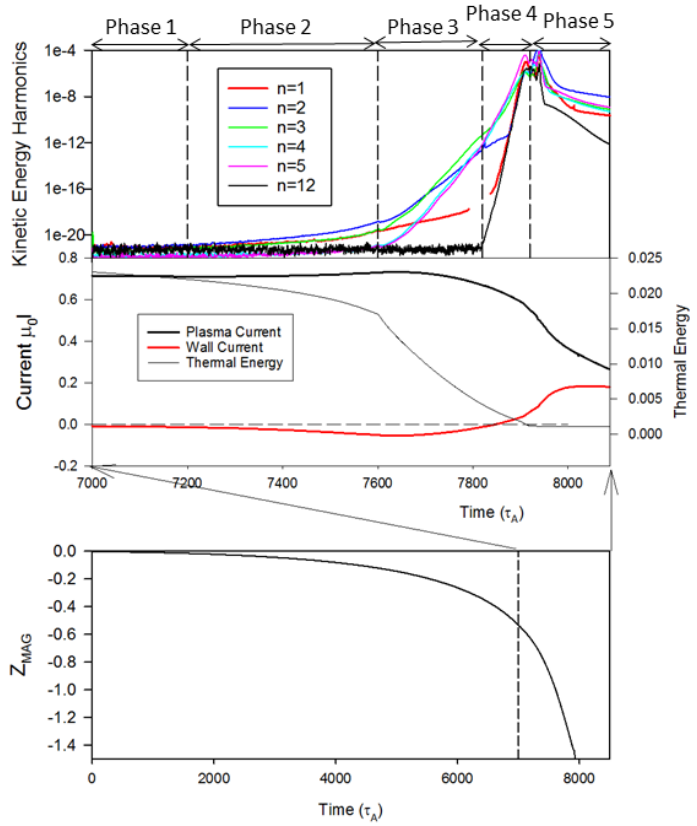

Figure 2: Bottom graph shows Z-position of magnetic axis vs time. At time t = 7000 τ_A the calculation was transferred from 2D to 3D. Top frame shows kinetic energy in different toroidal harmonics, and middle frame shows current in plasma and wall and thermal energy in plasma during the last 1000+ τ_A.

2.2 3D Vertical Displacement Event (VDE):

We have used the new resistive wall capability in M3D-C1 to model a fully 3D vertical displacement event in NSTX shot 132859. In these initial calculations, we have increased the vessel resistivity by a factor of 10 in order to ease computational requirements. A calculation with more realistic vessel resistivity will be presented elsewhere. [4]

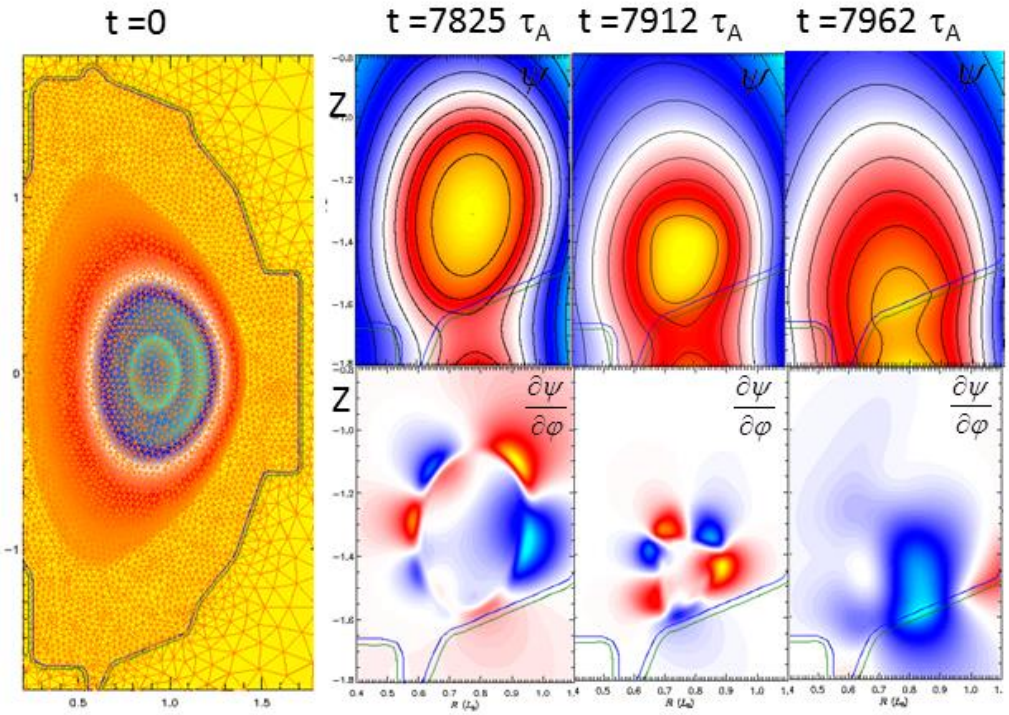

Figure 3: Leftmost figure shows initial toroidal current with superimposed mesh and vessel shown. Right figures show the poloidal flux ψ (top) and its toroidal derivative (bottom) at three times during the thermal quench.

Once vertical control is lost, the plasma drifts downward with the linear growth rate until it makes contact with the vessel and disrupts. The evolution goes through the five phases shown in Fig. 2. In the first phase, the plasma remains axisymmetric and just drifts downward at a nearly constant exponential rate. In Phase 2, a n=2 tearing mode starts to grow, joined by a n=3 tearing mode in Phase 3. In Phase 4, the n=1 external mode becomes strongly unstable and higher-n modes begin to grow as well. Finally, in Phase 5, the plasma gets scraped off by the wall and eventually disappears. During these phases, both inductive and halo currents are induced in the wall. The inductive current, shown in the middle frame in Fig. 3, is initially opposite in direction to the plasma current (to repel the plasma) but then switches to the same direction as the plasmas current as the plasma current decays. Forces from these induced and conductive currents will be given in [4]. Figure 3 illustrates the initial toroidal current (left) and the poloidal flux contours (right) at three times during the late phases of the VDE when the plasma is interacting with the lower vessel. Halo current flows along the contours closest to the plasma that intersect the vessel. The contours of the toroidal derivatives of the poloidal flux in the bottom frames show the poloidal mode structure.

2.3 Island Overlap Disruption:

We are participating in a nonlinear MHD benchmark exercise as part of the MHD ITPA known as JA-2. In the initial phase, we are looking at the nonlinear growth of magnetic islands in cylindrical equilibrium that initially have either one or two unstable tearing modes. Typical results are shown in Fig. 4 where we compare the island growth in a low-β

cylindrical equilibrium with 2 linearly unstable modes, (2,1) and(3,2), and with a safety factor profile: $q(r)=1.40\left[1+\left((r/a)^2/0.5476\right)^2\right]^{1/2}$, and an equilibrium unstable to a single (2,1) tearing mode with $q(r)=1.15\left[1+\left((r/a)^2/0.6561\right)\right]$. It is seen in Fig. 4 that the (2,1) island for the q_0=1.4 case grows to a much larger amplitude, and when the (3,2) island gets large enough, they interact to form a large stochastic region which would likely lead to a thermal quench and consequently full disruption. In contrast, the equilibrium with q_0=1.15 grows

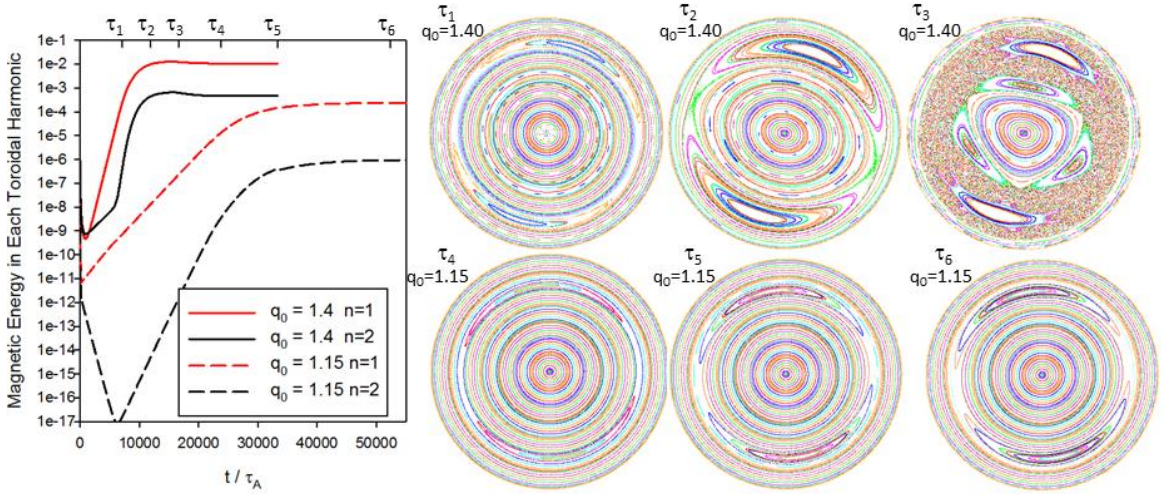

Figure 4: Comparison of evolution of cylindrical equilibrium with two unstable tearing modes (q_0=1.40, solid lines and top row) and with a single unstable tearing mode (q_0=1.15, dashed lines and bottom row)

to only about 15% of the minor radius and saturates without creating a stochastic region. These calculations used values of the Lundquist number of $S=10^5$ and Magnetic Prandtl number of P_M=1, with an aspect ratio of A=10. They are now being extended to include sheared toroidal rotation, toroidal geometry, and non-circular flux surfaces.

3.0 Soft limits:

3.1 Heating past the beta limit:

We have identified regions in parameter space where central heating of the plasma up to and beyond the ideal MHD beta limit does not lead to a disruption, but instead to increased transport which self-regulates the pressure increase [5]. Shown in Figure 5 is a NSTX plasma discharge 124379 at time 0.64 s. Increasing the central neutral beam heating causes an internal (4,3) mode to go unstable near the q = 1.33 surface. This instability distorts the magnetic surfaces in such a way that parallel thermal conductivity acts to reduce the pressure in the center of the discharge to the point where it becomes linearly stable and the magnetic surfaces reform. Figure 5 (upper) shows the Poincaré plots of the magnetic field and (lower) the incremental change in the electron temperature (from the start of the calculation) at four different

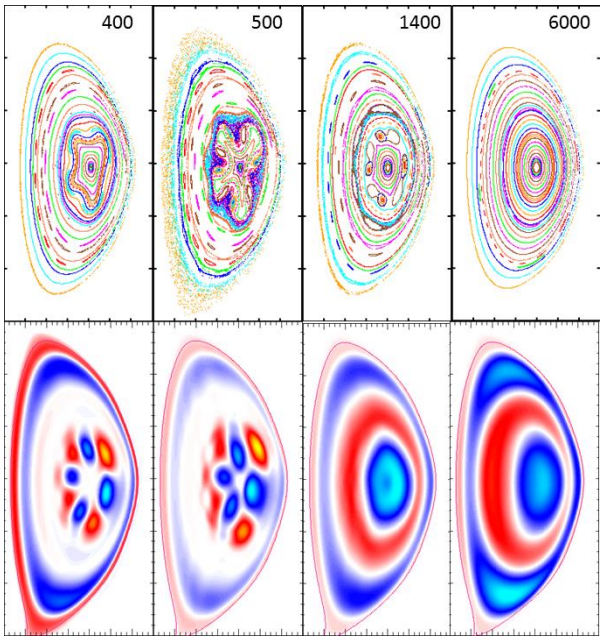

Figure 5: Poincare plots (top) and change in temperature (bottom) from the start of the calculation at 4 times.

times in the 3D calculation. It can be seen that the surfaces initially deform, then become stochastic in the center, but eventually completely heal and the configuration returns to axisymmetry to a high degree by the final time t=6000 τ_A.

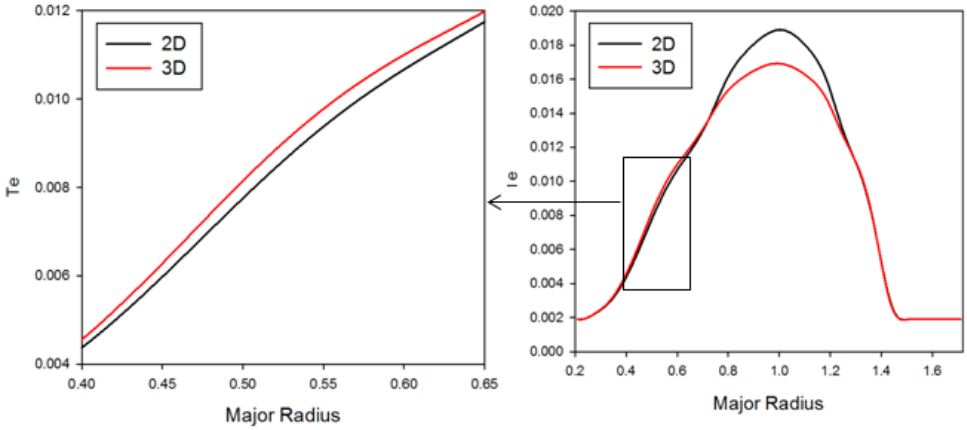

Figure 6: Mid-plane temperature at start and end of the calculation shown in Fig. 5. Energy is transferred from center to mid-radius

The perturbed temperature snapshots in Figure 5 show that initially a single mode grows up (n=3, m=4), and then nonlinearly couples to other modes, and finally the temperature re-symmetrizes and becomes constant on flux surfaces. (Note that because of the change in the shift of the magnetic axis, the final temperature snapshot shows in-out distortion). Figure 6 shows mid-plane profiles of the electron temperature at the final time for the fully 3D calculation and for a companion 2D calculation with the same (M3D-C1) code using exactly the same heating and transport coefficients but with axisymmetry maintained throughout (thus, making it 2D). It is seen that the effect of the 3D instability was to lower the temperature in the center, and to slightly raise the temperature at mid-radius, such that the integral of the thermal energy (as measured by β) stays unchanged from the 2D calculation. The net effect of the localized 3D MHD instability was to increase the effective thermal transport in the center of the discharge. This is an example of a soft β-limit.

3.2 Self-organized non-sawtoothing stationary states with q_0=1.

Tokamak discharges normally undergo sawtooth oscillations [7]. The kinetic energy in a β=0.06% simulation of a sawtoothing discharge is shown in Fig. 7 in red. However, for the same configuration, if we increase the β to 2%, the kinetic energy does not oscillate in time but reaches a stationary state with a non-zero kinetic energy as shown in the black curve in Fig. 7. We find that under certain conditions, and for sufficiently high plasma-β, the plasma can self-organize to produce a shear-free region in the center with q~1. This ultra-low shear configuration with q=1 is unstable to a (1,1) interchange mode [6]. This pressure-driven mode has several effects:

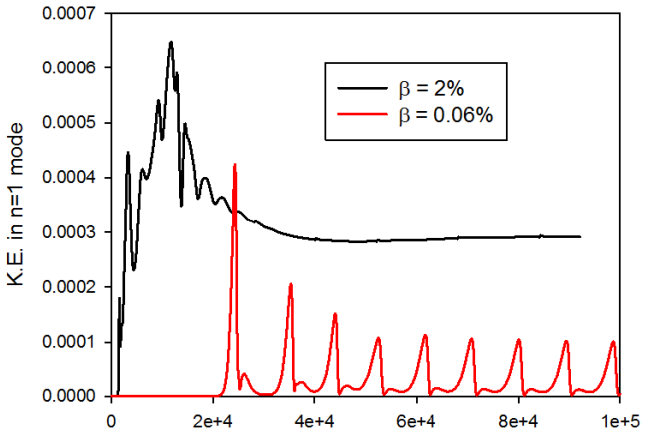

Figure 7: Kinetic energy vs time for a sawtoothing discharge (in red) and a non-sawtoothing stationary state with q0 = 1.

(i) It acts to reduce the central pressure by convection, (ii) it leads to a (1,1) component in the magnetic field in the center, and (iii) it leads to a stationary (1,1) electric potential Φ via $\nabla\Phi = \mathbf{V}\times\mathbf{B}$. The (1,1) component of the magnetic field and the (1,1) component of the electric potential combine together via $\mathbf{B}\cdot\nabla\Phi$ to nonlinearly generate a (0,0) dynamo voltage that prevents q_0 from decreasing further and thus sustains the configuration.

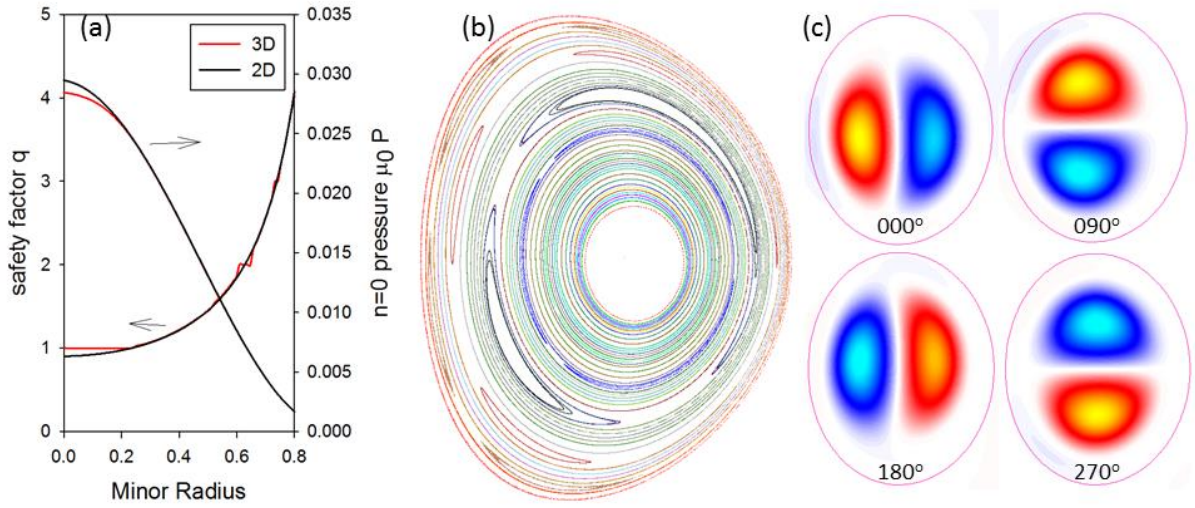

Figure 8: (a) shows the difference in the safety factor and pressure profiles for the 3D stationary state and a companion 2D calculation with the same transport coefficients. (b) shows a Poincaré plot of the stationary state, not showing the central region with q=1 where surfaces do not exist. (c) velocity potential contours in the central q=1 region at 4 different toroidal angles showing the (1,1) structure of the driven velocity field.

This (1,1) mode also causes other islands to form through toroidal and other mode coupling. This non-sawtoothing stationary state could explain "flux-pumping" the "hybrid" discharges in DIII-D [8] and other tokamaks. We are now extending our previous study [9] to include the effects sheared toroidal rotation, and to map out the region in parameter space where these stationary states are expected to occur.

3.3 *Edge-Localized modes:*

We have participated in a ELM benchmarking activity by modeling the evolution of KSTAR discharge #7328 at time t~4.36 s and comparing with other nonlinear codes and with experimental measurement [10]. Figure 9 shows the initial current (a) and the perturbed pressure at two times in the simulation using a uniform resistivity in the closed field-line region with $S=10^6$, dropping to S=1 in the open field line region. Figure 10 shows mid-plane profiles of the pressure at two times near the end of the calculation. It is clear that the ELM instability is highly localized to the plasma edge, reducing the edge pressure gradient and sending blobs of plasma out to the open-field line region, leaving the pressure in the core region of the plasma unaffected. This appears to be in contrast to some earlier published ELM simulations where the perturbation extends far into the plasma core [11].

We are now extending these simulations to NSTX plasmas and to include Lithium pellet injection, showing that injection of Lithium pellets into a pedestal near marginal stability can trigger an edge localized mode (ELM) without further disrupting the discharge [12].

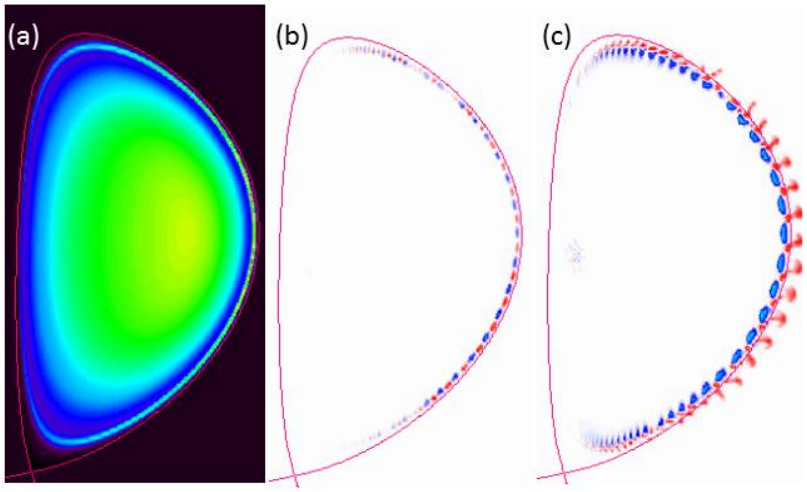

Figure 9: (a) Toroidal current density at time 0, (b) Perturbed pressure at time t=180 τ_A, (c) Perturbed pressure at time t=360 τ_A (colors normalized to maximum value at that time).

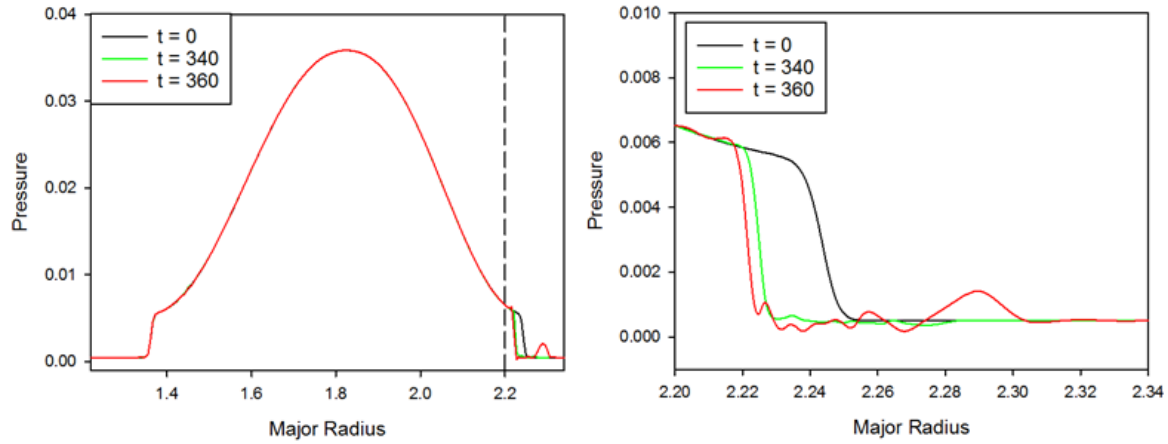

Figure 10: Mid-plane pressure profile at three times for calculation presented in Figure 9.

4.0 Concluding Remarks

The concept of using stability maps or real-time linear stability analysis to avoid disruptions needs to be informed by the likelihood that crossing a linear stability boundary leads to a disruption. The present work is a step in providing that information. The examples of instabilities given in Sec. 3.1, 3.2, and 3.3 are those of configurations that do become linearly unstable to ideal or resistive MHD modes but that are self-regulating and do not lead directly to a disruption. The examples we showed of instabilities that lead to a disruption involve either free-boundary instabilities or overlapping magnetic islands. Future work with the nonlinear MHD stability code M3D-C1 will include investigating instabilities involving mode-locking, and more generally will seek to find criteria to distinguish catastrophic vs non-catastrophic instabilities. The longer term goal is to better understand the sequence of events that lead to a plasma disruption, and to identify regimes that are less disruption-prone.

Acknowledgements: This work was supported by US DOE Contract NO. DE-AC02-09CH11466 , the SciDAC Center for Extended Magnetohydrodynamic Modeling, and the Max-Planck Princeton Center for Plasma Physics. The authors thank M. Kim and H. Park for providing them with the equilibrium used in Section 3.3

References:

[1] JARDIN, S.C., FERRARO, N.M., BRESLAU, J., CHEN,J., "Multiple timescale calculations of sawteeth and other global macroscopic dynamics of tokamak plasmas", Computational Science and Discovery **5** (2012) 014002.

[2] ZHANG, F., HAGER, R., KU, S., et al., "Mesh generation for confined fusion plasma simulation", Engineering with Computers **32** (2016) 285-293

[3] FERRARO, N.M., JARDIN, S.C., LAO, L.L., et al., "Multi-region approach to free-boundary three-dimensional tokamak equilibria and resistive wall instabilities", Physics of Plasmas **23** (2016) 056114

[4] PFEFFERLE, D., FERRARO, N., JARDIN, S., BHATTACHARGEE, A., "Fully 3D modeling of tokamak vertical displacement events with realistic parameters", Bull. Am. Phys. Soc. GP10.00086 (2016)

[5] BRESLAU, J., CHEN, J., FERRARO, N., et al. "Nonlinear Calculations of Soft and Hard Beta limits in NSTX", Proceedings of the 40th EPS Conference on Plasma Physics, Finland (2013) Available online: ocs.ciemat.es/EPS2013PAP/html

[6] HASTIE, R.J. and HENDER, T.C. "Toroidal Internal Kink Stability in Tokamaks with Ultra Flat q Profiles", Nuclear. Fusion **28** (1988) 585

[7] VON GOELER, S., STODIEK, W., SAUTHOFF, N., "Studies of Internal Disruptions and m=1 Oscillations in Tokamak Discharges with Soft-X-Ray Techniques, Phys. Rev. Lett., **33** (1974) 1201

[8] PETTY, C.C., AUSTIN, M.E., HOLCOMB, C.T., "Magnetic-Flux Pumping in High-Performance, Stationary Plasmas with Tearing Modes", Phys. Rev. Lett. **102** (2009) 045005

[9] JARDIN, S.C., FERRARO, N.M., KREBS, I., "Self-Organized Stationary States of Tokamaks", Phys. Rev. Lett. **115**, (2015) 215001

[10] KIM, M., LEE, J., LEE, J.E., PARK, H. K., et al. "Study of Nonlinear Phase of the ELMs by Comparison between ECEI ELM Observation and Nonlinear MHD Simulations", EX/P4-7, ibid (2016)

[11] SUGIYAMA, L.E., STRAUSS, H.R., "Magnetic X-points, edge localized modes, and stochasticity", Phys. Plasmas. **17** (2010) 062505

[12] FIL, A., KOLEMEN, E., FERRARO, N., JARDIN, S., et al, "Modeling and Simulation of Pedestal Control Technique for NSTX-U", TH/P1-10, ibid (2016)